Preprint of L. Boeck, M. Meijers, A. Kink, R. Mével, and J. E. Shepherd.
Ignition of fuel-air mixtures from a hot circular cylinder.
Combustion and Flame, 185:265-277, 2017. Final version available at
https://doi.org/10.1016/j.combustflame.2017.07.007.

Ignition of fuel-air mixtures from a hot circular cylinder

L.R. Boeck[a], M. Meijers[b], A. Kink[c], R. Mével[a,d,e], J.E. Shepherd[a]

[a] *Graduate Aerospace Laboratories, California Institute of Technology, Pasadena, CA 91125, USA*
[b] *École Polytechnique, 91128 Palaiseau Cedex, France*
[c] *Technische Universität München, 85747 Garching, Germany*
[d] *Center for Combustion Energy, Tsinghua University, Beijing 100084, China*
[e] *Department of Automotive Engineering, Tsinghua University, Beijing 100084, China*

Abstract

Ignition of hydrogen-air, ethylene-air and n-hexane-air mixtures from a horizontally and vertically oriented heated circular cylinder was studied experimentally in a wide range of equivalence ratio. Initial pressure and temperature were 101.3 kPa and 296 K, respectively. The cylinder with outer diameter 10 mm and heated length 10 mm was designed for high temperature uniformity. Two-color pyrometry measured the surface temperature; Time-resolved Mach-Zehnder interferometry acquired ignition dynamics, gas temperature fields and heat transfer characteristics. Ignition from the horizontal cylinder occurred at temperatures between 960 K and 1100 K for hydrogen, between 1060 K and 1110 K for ethylene, and between 1150 K and 1190 K for n-hexane. Vertical cylinder orientation increased ignition thresholds by 50–110 K for ethylene and n-hexane, whereas only little variation was observed for hydrogen. Infinite-fringe interferograms visualized the ignition dynamics and identified the most favorable ignition locations, which coincided with locations of lowest wall heat flux (largest

*Corresponding author. Current affiliation: L.R. Boeck, FM Global, Research Division, 1151 Boston-Providence Turnpike, Norwood, MA 02062, lorenz.boeck@fmglobal.com

thermal boundary layer thickness) and long residence time. Gas temperature fields were obtained by post-processing the interferograms, resolving the temporal and spatial development of thermal boundary layers and enabling local heat transfer analysis. The convective pattern around a horizontal cylinder features distinctly shallow temperature gradients, i.e., low heat flux, at the cylinder top due to thermal plume formation, which promotes ignition compared to the vertical cylinder. An analytical scaling model for ignition from hot surfaces was evaluated to determine the sensitivity of ignition threshold to heat transfer variations, and to reveal the influence of chemical mixture properties. This analysis predicts a particularly low sensitivity for hydrogen-air mixtures at temperatures near the extended second explosion limit, and a larger sensitivity of ethylene-air and n-hexane-air mixtures, which is in accordance with the experiments.
Keywords: hot surface ignition, cylinder, interferometry, heat transfer

---

1. Introduction

Ignition of reactive gas mixtures from hot surfaces constitutes a hazard in many industries. Parameters such as surface size, shape, material and heating rate affect the minimum surface temperature required for ignition, referred to as the ignition threshold. For a given hot object and heating rate, the ignition threshold is a function of gas mixture composition, initial thermodynamic state of the gas and the flow regime, i.e., whether the gas is initially quiescent or an external flow is present. The present paper focuses on localized hot surfaces located in a large volume of reactive mixture, in contrast to ignition from extended surfaces such as heated vessels. Ignition from localized hot surfaces which are not catalytic is dominated by the formation of a thermal boundary layer around the hot object and the competition between energy release and creation of reactive species from chemical reactions within the boundary layer and transport processes to the surface.

Literature on hot surface ignition spans several decades and there is a sub-

stantial body of empirical data that primarily focuses on critical temperatures for ignition and simplified analytical models. Rapidly heated wires with sub-millimeter diameters represent a classical experiment [1–16]. Rapid energy deposition into the wire leads to the separation of time scales for wire heating, thermal conduction into the gas and chemical reaction, and the temperature field can be treated as quasi one-dimensional in the limit of fast heating. Experiments on rods with millimeter-diameters [6, 17–19] and heated foils [20–22] extended the range of surface sizes. Ignition from hot particles was investigated by [23–33]. Two trends emerge from the experimental studies: Larger hot surfaces enable lower ignition thresholds, and quiescent initial conditions enable lower ignition thresholds compared to situations where external flow is present. The analytical studies have emphasized explaining these trends by balancing energy generation with heat losses to surfaces to predict ignition temperatures.

The accuracy of ignition experiments depends on the hot surface used and on the type of diagnostics [20, 21]. The uniformity of surface temperature needs to be optimized and quantified to reduce uncertainties. The present study extends previous work that used a commercial glow plug as a hot surface [34–39]. To improve the surface temperature uniformity, a new cylindrical surface was developed with a unity aspect ratio of the hot surface section. Horizontal and vertical cylinder orientations were tested to examine the role of heat transfer variations on ignition thresholds. Heating times from ambient temperature to ignition temperature longer than 40 s allowed natural convection to fully develop, i.e., the flow field adapted quasi-instantaneously to changes in surface temperature, which distinguishes the present study from rapid heating experiments. Results in terms of ignition thresholds, ignition dynamics and heat transfer were obtained for hydrogen-air, ethylene-air and n-hexane-air mixtures in a wide range of equivalence ratio at an initial pressure of 101.3 ± 0.1 kPa and initial temperature of 296 ± 3 K. An analytical scaling model is applied to further study the effect of local heat transfer, surface orientation and chemical mixture properties on ignition thresholds.

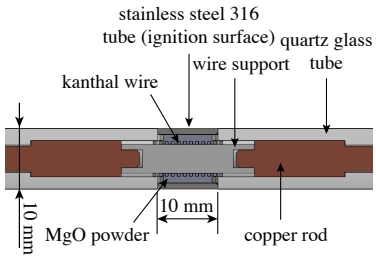

Figure 1: Cross-sectional view of the heated cylinder.

2. Experimental setup

2.1. Combustion vessel

Ignition experiments were performed in a 2.2 L closed prismatic vessel with internal dimensions 0.114 m × 0.114 m × 0.165 m. The vessel was evacuated to below 10 Pa and filled with fuel, oxygen and nitrogen using the method of partial pressures with a 10 Pa accuracy. The gases were mixed by a circulation pump and left to settle for 3 minutes to ensure quiescent initial conditions. Initial pressure and temperature before the start of the surface heating were 101.3 ± 0.1 kPa and 296 ± 3 K, respectively. Gaseous fuels, i.e., hydrogen and ethylene, were supplied from gas cylinders and liquid fuel, i.e., n-hexane, was injected as a liquid and evaporated. The vessel was equipped with lateral viewing windows providing optical access for pyrometric and interferometric measurements.

2.2. Heated cylinder

A well-defined experiment on hot surface ignition demands a hot surface with small spatial variations in temperature. Especially for small surfaces, this poses a design challenge. Non-uniformity in temperature may affect the development of natural convection and chemical activity. Likewise, a local measurement of surface temperature may not represent the actual surface temperature at the location of ignition.

A stainless steel (316) cylinder heated internally by a Kanthal A-1 FeCrAl alloy resistance heating wire subjected to electric current was selected as a hot

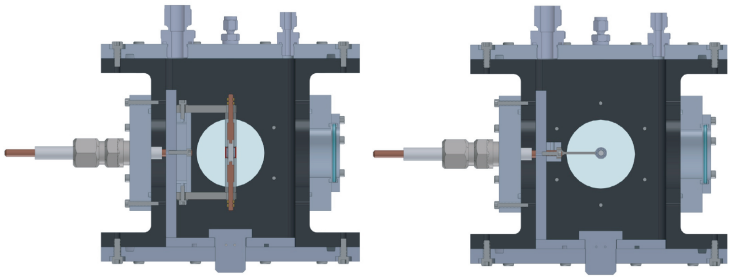

Figure 2: Combustion vessel with heated cylinder mounted vertically (left) and horizontally (right).

surface in the present study. The dimensions of the hot surface were $D = 10\,\text{mm}$ outer diameter, $L = 10\,\text{mm}$ length (aspect ratio $L/D = 1$), and $d = 1\,\text{mm}$ wall thickness. Figure 1 presents a cross-sectional view of the device. The material, stainless steel (316), corresponds to previous work using a commercial glow plug as a hot surface [34–37, 39]. The stainless steel tube was centered between two 30 mm long thermally and electrically insulating quartz glass tubes to create a continuous geometric contour and to limit axial heat loss. Compacted magnesium oxide powder filled the internal gap between the heating wire and the stainless steel tube, providing electrical insulation and high thermal conductivity [40]. Copper rods and attached cabling connected the heating wire to a constant electrical current source. The cylinder was mounted in the center of the combustion vessel. Both vertical and horizontal cylinder orientations were examined, see Fig. 2.

3. Diagnostics

3.1. Two-color pyrometry

The hot surface temperature was measured by two-color pyrometry. Near-infrared radiation emitted from the stainless steel surface was collected through a 75 mm focusing lens positioned at a distance of 140 mm and directed towards two InGaAs detectors (Thorlabs PDA10DT) by a dichroic beam splitter with a cut-off wavelength of 1800 nm. The focusing lens was made of uncoated N-BK7

with a high transmission between 350 nm and 2.0 μm and a design wavelength of 587.6 nm. Focal shift due to chromatic aberration was compensated by adjusting the detector positions. The two detectors were equipped with a different bandpass filter each with central wavelengths 1705 nm and 1940 nm and FWHM 97 nm and 105 nm, respectively. The ratio of bandpass-filtered radiation intensities, I_1/I_2, correlates with the surface temperature T_S. For narrow filter bandwidths and assuming gray-body emission from the hot surface, T_S was determined by the equation

$$ln\left(\frac{I_1}{I_2}\right) = \frac{A}{T_S} + B, \tag{1}$$

where constants A and B were obtained through calibration using a black-body radiation source (Process Sensors BBS1200). Temperature measurement uncertainty due to the wavelength-dependence of emissivity for real surfaces was quantified according to [41]. In addition, uncertainties due to measurement noise and calibration source uncertainty were taken into account. On average, the uncertainties amount to 4-5% in temperature and will be represented by error bars.

The pyrometer field-of-view was characterized by collecting radiation from the black body through apertures of different diameters. Irradiance was assumed constant across the black body, so that a sensitivity profile for each detector could be obtained. Sensitivity profiles were found to be Gaussian for the 1705 nm and 1940 nm wavelengths with FWHM 1.006 mm and 1.022 mm and $1/e^2$-diameters 1.698 mm and 1.726 mm, respectively. Due to the chromatic shift compensation, the sensitivity profile widths were nearly identical for both wavelengths.

In a preliminary study, scanning pyrometry was performed to characterize the surface temperature uniformity by translating the pyrometer along the heated cylinder axis using a closed-loop controlled stepper motor. Bi-directional scans with an axial speed of 12.7 mm/s and the assumption of linear heating

during this period enabled the acquisition of surface temperature profiles during transient surface heating. During the ignition experiments, the pyrometer field-of-view remained fixed at the center of the stainless steel tube. This location coincided with the location of maximum surface temperature.

The pyrometer detector voltages were recorded with digital storage oscilloscopes (Pico Technology PicoScope and LeCroy Wavesurfer 44 MXs).

3.2. Mach-Zehnder interferometry

Time-resolved Mach-Zehnder interferometry was applied to measure the refractive-index variations in the gas surrounding the hot surface, observe the ignition event and infer temperature fields and heat transfer parameters. A 532 nm beam from a Spectra-Physics Excelsior-532-200-CDRM laser was expanded to form a planar wavefront and split by a prismatic beam splitter into the measurement beam and the reference beam. The former passed through the combustion vessel, and the latter was directed around the vessel. Both beams were recombined in a second prismatic beam splitter forming an interference pattern which was recorded by a Phantom V7-11 high-speed camera. Both finite and infinite-fringe interferograms were obtained.

Variations of gas density ρ inside the combustion vessel result in variations of refractive index n, which is described by the Lorenz-Lorentz equation in the present work [42],

$$\langle R_L \rangle = \frac{n^2 - 1}{n^2 + 2} \cdot \frac{W}{\rho}, \tag{2}$$

where $\langle R_L \rangle$ and W are the molar refractivity and the molar mass of the mixture, respectively.

The molar refractivity of a gas mixture $\langle R_L \rangle$ is given by the refractivities of the mixture components $R_{L,i}$ and their mole fractions X_i, $\langle R_L \rangle = \sum_{i=1}^{N} R_{L,i} X_i$. Refractivities $R_{L,i}$ of mixture components were taken from [43]. For gases

($n \approx 1$), the empirical Gladstone-Dale law, $R_{GD} = W(n-1)/\rho$, agrees well with experimental data. R_{GD} is the Gladstone and Dale molar refractivity, which is $R_{GD} \approx 3R_L/2$ for gases. Either relationship can be used in practice to establish the relationship between n and ρ [44].

Rays of light with wavelength λ propagate through the vessel volume along the z-axis and accumulate an optical path length difference $\Delta\phi$ due to variations of refractive index $n(z)$ compared to the refractive index at initial conditions n_0. In the refractionless limit, that is, light propagates along straight lines, the vessel volume, extending from ξ_1 to ξ_2, is treated as a phase object and the optical phase difference $\Delta\varphi = \Delta\phi \cdot (2\pi/\lambda)$ can be written [42] as

$$\Delta\varphi = \frac{2\pi}{\lambda} \int_{\xi_1}^{\xi_2} [n(z) - n_0] \, \mathrm{d}z. \tag{3}$$

Neglecting refraction effects is reasonable during the surface heating period before a flame is established [44]. The recorded intensity pattern $I(x, y)$ of a finite-fringe interferogram is interpreted as a modulated function [45],

$$I\,(x, y) = a\,(x, y) + b\,(x, y) \cos \Delta\varphi\,(x, y)\,, \tag{4}$$

where a represents background signal and noise and b is the signal amplitude. The optical phase difference was recovered from finite-fringe interferograms by two-dimensional Windowed Fourier Transformation and phase unwrapping [31, 46–48]. Infinite-fringe interferograms can be evaluated directly by determining the fringe locations characterized by intensity extrema. Each fringe represents a contour of optical phase difference, adjacent fringes are separated by an optical phase difference of π.

In the case of vertical cylinder orientation, axial symmetry of the refractive-index fields allowed for inverting Eq. (3). The numerical method by Pretzler [49] was adopted to perform the Abel inversion and to recover the two-dimensional

refractive-index fields in the cylinder center plane. From Eq. (2), the gas density was computed, and temperature was determined from the ideal gas law.

Heat transfer into the quartz glass support cylinders, see Sec. 5.3, complicated the interferogram interpretation for the horizontal cylinder orientation. The temperature and flow fields are expected to be three-dimensional. Only for an ideally planar situation without any heat transfer into the quartz glass cylinders we could assume a constant refractive index along the cylinder axis and determine the refractive-index field directly from $n(x,y) = n_0(x,y) + \Delta\varphi(x,y)/(\xi_2 - \xi_1)$, where $(\xi_2 - \xi_1)$ would be the length of the stainless steel cylinder L. In heat transfer studies such a situation is commonly established by a large aspect ratio L/D of the cylinder. For our case, $L/D = 1$, we can still obtain qualitative results: Instead of imposing a geometric path length, we determined the effective geometric path length $L_{geo,eff}$ such that the gas temperature inferred from interferograms at the cylinder surface matched the surface temperature measured simultaneously by pyrometry. Hence, the refractive-index field was obtained from $n(x,y) = n_0(x,y) + \Delta\varphi(x,y)/L_{geo,eff}$.

4. Characteristics of heating process and hot surface

The temporal evolution of surface temperature during heating of the horizontal cylinder is presented in Fig. 3 for stoichiometric fuel-air mixtures. At surface temperatures below about 700 K, a low signal-to-noise ratio due to low radiation intensity prevented meaningful surface temperature measurements. At the individual times of ignition, clear spikes can be seen in the temperature curves. The pyrometer readings after ignition, showing an unphysical decrease, were influenced by the presence of the flame and do not represent actual surface temperatures. At the individual times of ignition, heating rates were low, 2–10 K s^{-1}. The pressure and bulk temperature increase inside the vessel from the beginning of surface heating to the instant shortly before ignition was below 4% in all experiments.

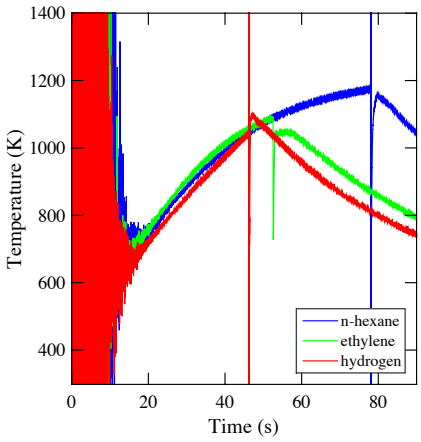

Figure 3: Temperature of the horizontal cylinder surface as a function of time elapsed since the beginning of heating measured by pyrometry for stoichiometric fuel/air mixtures.

Such heating rates are sufficiently low for the gas temperature field to adapt quasi-instantaneously to the evolution of surface temperature. This aspect differentiates the present work from rapid heating experiments. Ignition takes place in close proximity to the surface within the thermal boundary layer. The characteristic time for the thermal boundary layer to adapt to a change in surface temperature may be estimated by the relaxation time for thermal conduction [50], $\tau \approx \delta_{99}^2/\alpha$, where δ_{99} is the thermal boundary layer thickness and α is thermal diffusivity. For a stoichiometric hydrogen-air mixture, δ_{99} ranges around 6–8 mm in conduction-dominated regions at a surface temperature $T_S = 1000\,\mathrm{K}$, see Sec. 5.3. Evaluating α at film temperature, $T_F = (T_S - T_0)/2$, τ is on the order of 0.3–0.5 s. For heating rates at the time of ignition of 2–10 K s^{-1} transient effects of surface heating on the temperature field may be considered small.

The spatial temperature distribution across the stainless steel tube during transient heating was measured by means of scanning pyrometry. Figure 4 presents temperature as a function of axial location y for different times during

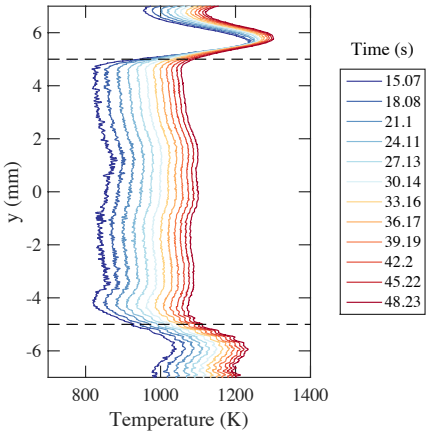

Figure 4: Surface temperature profiles along the cylinder during heating in air, measured by scanning pyrometry. Horizontal dashed lines mark boundaries of the heated stainless steel cylinder at $y = \pm 5mm$.

a heating process in air. Coordinates $y \in [-5\,\mathrm{mm}, 5\,\mathrm{mm}]$ refer to the location relative to the center of the heated stainless steel surface. Outside of this region radiation from the internal heating wire was transmitted through the quartz glass support cylinders and registered by the pyrometer. Hence, these temperatures do not represent valid surface temperatures. For $y \in [-4.5\,\mathrm{mm}, 4.5\,\mathrm{mm}]$, we expect valid measurements. The temperature reaches a maximum near the center, $y = 0\,\mathrm{mm}$, and decreases by less than 3% towards the metal surface edges. This temperature variation is considered reasonably small given the dimensions of the hot surface and is an improvement over previous experiments using a commercial glow plug with temperature variations of up to 10% across its 9.3 mm height [39].

5. Experimental results

This section presents the experimental results, which will be interpreted afterwards in detail in Sec. 6.

5.1. Ignition thresholds

Temperatures of the hot surface measured by two-color pyrometry at the time of ignition (ignition thresholds), signified by a discontinuity in the temperature reading (see Fig. 3), are reported for horizontal and vertical cylinder orientation. Experimental repeatability tests were conducted only for specific conditions due to the large number of conditions that were tested. For most conditions, high repeatability was observed. For example, ignition thresholds for the horizontal cylinder and stoichiometric hydrogen-air mixture were 1051 K, 1055 K and 1046 K in three experiments at identical nominal conditions. Except for one configuration (vertical cylinder, hydrogen-air mixtures), the measurement uncertainty clearly exceeded the variations observed between repeated tests.

Ignition thresholds for stoichiometric fuel-air mixtures are presented in Fig. 5 along with auto-ignition temperatures (AIT) from literature [51] for comparison. Error bars include measurement uncertainties and variations between three repeated tests for each fuel. Overall, the stoichiometric hydrogen-air mixture showed the lowest thresholds, followed by ethylene-air and n-hexane-air. Hydrogen-air ignition thresholds were nearly independent of cylinder orientation, and ranged around 1050 K. Thresholds for ethylene-air and n-hexane-air mixtures showed a dependency on cylinder orientation: For both fuels, thresholds were higher for the vertical orientation than for horizontal. Stoichiometric ethylene-air mixture ignited at about 1090 K from the horizontal cylinder and at about 1180 K from the vertical cylinder; stoichiometric n-hexane-air mixture ignited at about 1180 K from the horizontal cylinder and at about 1270 K from the vertical cylinder.

All thresholds for ignition from the present hot surface are distinctly higher than AITs determined in extended hot vessels, which is consistent with previous data on hot surface size effects [4]. In addition, it is interesting to note the qualitatively different trends in AIT and hot surface ignition thresholds between the three fuels. AITs decrease from hydrogen-air towards ethylene-air and

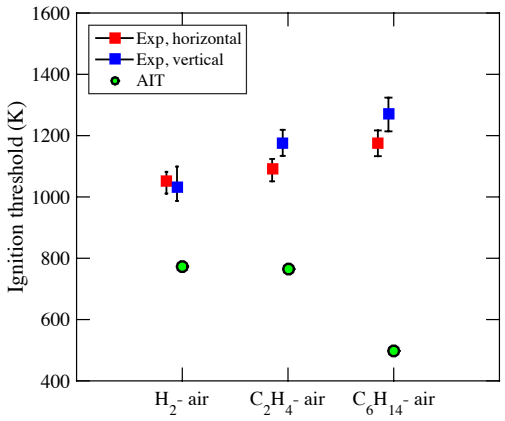

Figure 5: Ignition thresholds of stoichiometric fuel-air mixtures. Initial pressure and temperature 101.3 kPa and 296 K, respectively. Auto-ignition temperatures (AIT) from [51].

n-hexane-air, whereas the hot surface ignition thresholds increase. Additional work is required to understand this effect in detail. In particular, evaluating the dominant chemical pathways at high and low temperatures representative of hot surface ignition temperatures and AIT conditions, respectively, might yield further insight.

Figure 6 presents ignition thresholds for the horizontal cylinder orientation as a function of fuel mole fraction. Red symbols mark ignition events, black symbols denote no-ignition cases. For the latter, the maximum surface temperature reached during the experiment is reported. Hydrogen-air mixtures showed an increase in ignition threshold from 960 K to 1100 K with increasing hydrogen mole fraction; Ignition thresholds for ethylene-air decreased from 1110 K to 1060 K with increasing ethylene mole fraction; Ignition thresholds for n-hexane-air ranged between 1150 K and 1190 K.

Ignition thresholds measured for the vertical cylinder orientation are given in Fig. 7. Hydrogen-air mixtures showed an increase in ignition threshold from 980 K to 1115 K with increasing hydrogen mole fraction. Increased variabil-

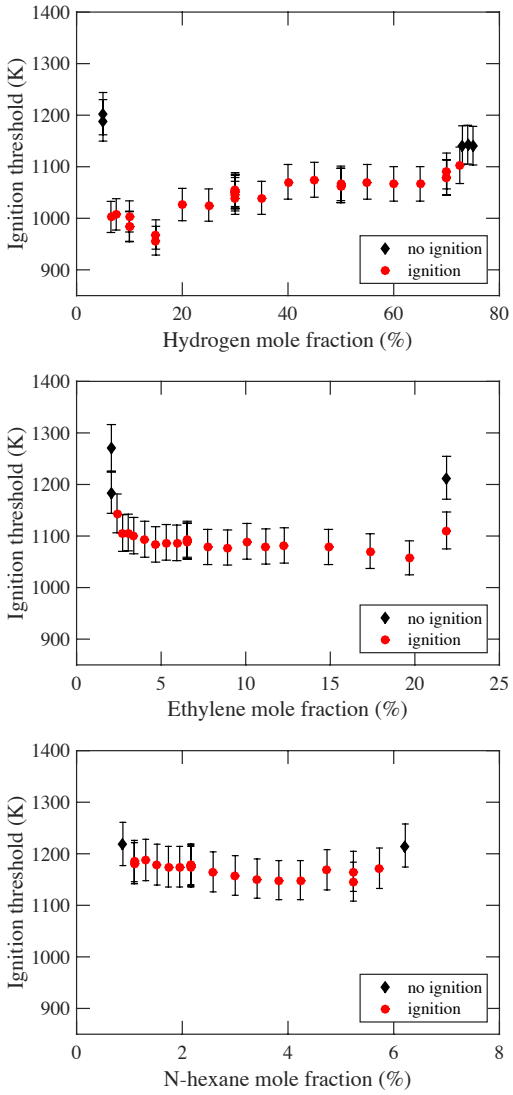

Figure 6: Ignition thresholds of the horizontally oriented cylinder as a function of equivalence ratio. Initial pressure and temperature 101.3 kPa and 296 K, respectively.

ity occurred at hydrogen mole fractions around 40%. Ethylene-air thresholds ranged between 1160 K and 1210 K, and thresholds for n-hexane-air mixtures ranged between 1250 K and 1260 K. Note that the maximum surface temperature achievable with the heated cylinder without damaging the quartz glass parts was about 1270–1280 K. For the cases reported as no-ignition, heating to higher temperatures might result in ignition, but we did not attempt to determine if this is the case.

Comparing the horizontal and vertical cylinder orientation across a wide range of equivalence ratio, ignition thresholds of hydrogen-air mixtures were rather insensitive to cylinder orientation. Both ethylene-air and n-hexane-air mixtures demonstrated higher ignition thresholds in the vertical cylinder configuration than in the horizontal.

5.2. Ignition dynamics

Mach-Zehnder interferometry was applied to experiments with hydrogen-air mixtures and is used here to examine ignition dynamics for a stoichiometric mixture. Raw infinite-fringe interferograms are shown rather than processed images since the localized appearance of a fast-propagating flame complicates post-processing and may violate symmetry assumptions.

Figure 8 presents the ignition event for the horizontal cylinder configuration recorded at 7500 fps. Each fringe represents a contour on line-of-sight integrated optical phase difference, which would correspond to a contour of density or temperature in an ideally planar geometry. Concentric fringes below the cylinder equator, $-180^\circ < \theta < 0^\circ$, indicate that quasi one-dimensional heat conduction dominated the temperature field in this section. Above the equator, $0^\circ < \theta < 180^\circ$, natural convection formed a thermal plume. A flame kernel developed at the top of the cylinder at $t_{ign} = 46.22$ s, visualized by a dashed red contour, which was added manually based on careful inspection of fringe deflection. The conditions are most favorable for ignition at this location as

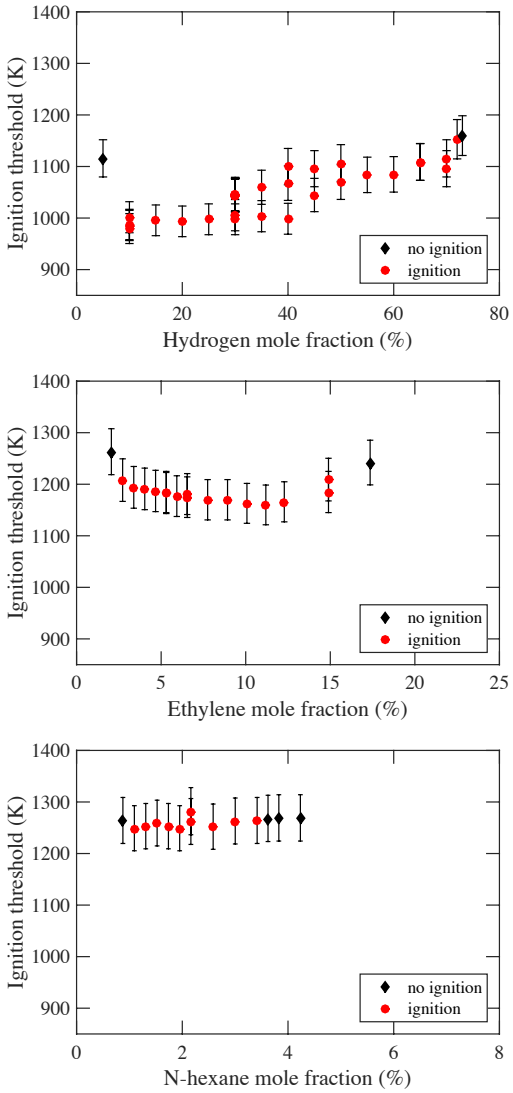

Figure 7: Ignition thresholds of the vertically oriented cylinder as a function of equivalence ratio. Initial pressure and temperature 101.3 kPa and 296 K, respectively. Ignition limits in terms of concentration for n-hexane-air are likely dominated by limited hot surface heating capabilities.

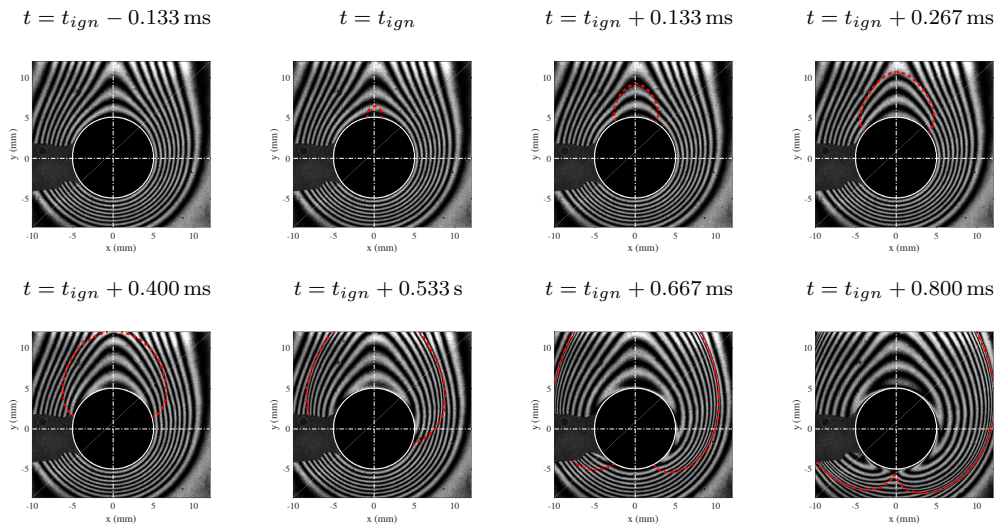

Figure 8: Infinite-fringe interferograms recorded at 7500 fps showing ignition from the horizontal cylinder in a stoichiometric hydrogen-air mixture. Time of ignition $t_{ign} = 46.22\,\mathrm{s}$. Red dashed lines visualize the flame front.

will be explained later. The flame propagated preferentially upward along the thermal plume at a mean velocity of about 30 m/s, but also circumferentially along the cylinder surface at a mean velocity of about 20 m/s as evaluated at the cylinder surface. Note that these observed flame speeds cannot be directly compared to laminar flame speed measurements due to the presence of hot reactants within the thermal boundary layer, the presence of buoyancy-driven flow and local flame curvature effects. Flame fronts propagating along the right- and left-hand sides of the cylinder merged at the cylinder bottom at $t_{ign} + 0.800\,\mathrm{ms}$ and detached from the cylinder surface subsequently.

Figure 9 shows the ignition event for the vertical cylinder orientation. In this configuration the flame causes clearly visible fringe deflection, so that additional visualization by red lines is not needed. Qualitatively, the expansion of fringes from bottom to top at $t_{ign} - 0.133\,\mathrm{ms}$ indicates the growth of thermal boundary layer in the vertical direction, which will be evaluated in more detail in the following section. Since the refractive-index field is axisymmetric, the location of

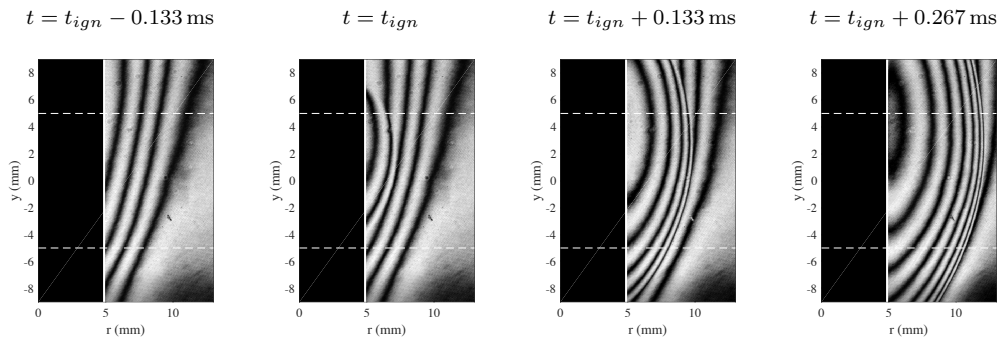

Figure 9: Infinite-fringe interferograms recorded at 7500 fps showing ignition from the vertical cylinder in a stoichiometric hydrogen-air mixture. Time of ignition $t_{ign} = 45.10\,\mathrm{s}$. Horizontal dashed lines mark boundaries of the heated stainless steel cylinder at $y = \pm 5mm$.

fringes results from line-of-sight integration, and fringes are no longer contours of density or temperature. For further analysis such fields need to be Abel-inverted. Ignition was observed at $t_{ign} = 45.10\,\mathrm{s}$ and $y \approx 4\,\mathrm{mm}$. The circumferential ignition location varied randomly between experiments, which indicates high circumferential surface temperature uniformity.

5.3. Gas temperature fields and heat transfer

For the horizontal cylinder, we inferred the optical phase difference fields from finite-fringe interferograms and obtained temperature fields by following the procedure described in Sec. 3.2. For the present small aspect ratio of the heated cylinder section, $L/D = 1$, a substantial quantitative uncertainty is anticipated due to three-dimensional flow, and the analysis is considered mostly qualitative. Figure 10 shows temperature fields at given surface temperatures for a stoichiometric hydrogen-air mixture along with temperature profiles in radial coordinates for the case of surface temperature $T_S = 1000\,\mathrm{K}$. The azimuthal angles corresponding to these temperature profiles are indicated with dashed lines in the corresponding temperature field. Below the equator, $-90° < \theta < 0°$, temperature profiles were similar, which confirms the dominance of quasi one-dimensional heat conduction in this region. The thermal boundary layer thickness was $\delta_{99} \approx 6.7\,\mathrm{mm}$ at $T_S = 1000\,\mathrm{K}$ and $\theta = -90°$. Above the equator, $0° < \theta < 90°$, the formation of a thermal plume led to a strong increase in

thermal boundary layer thickness exceeding the field-of-view. At the cylinder top, $\theta = 90°$, the smallest temperature gradient appeared. Shallow temperature gradients promote ignition as Sec. 6.2 will discuss in more detail. The normalized temperature gradient at the cylinder surface is shown in Fig. 11. The evolution as a function of angle is in qualitative agreement with the well-established literature on natural convection from horizontal circular cylinders as summarized in [52].

Abel inversion of optical phase difference fields for the vertically oriented cylinder yielded quantitative temperature fields in the cylinder center plane during surface heating. Figure 12 shows temperature fields corresponding to surface temperatures $T_S = [800\,\mathrm{K}; 900\,\mathrm{K}; 1000\,\mathrm{K}]$ and temperature profiles at $T_S = 1000\,\mathrm{K}$ and selected heights y. The heated stainless steel cylinder is located at $-5\,\mathrm{mm} < y < 5\,\mathrm{mm}$. Note that temperature profiles at $y = 4\,\mathrm{mm}$ and 6 mm show inaccuracies close to the cylinder surface, $5\,\mathrm{mm} < r < 6\,\mathrm{mm}$, leading to under-prediction of the surface temperature. At $T_S = 1000K$, the thermal boundary layer thickness was $\delta_{99} = 8.2\,\mathrm{mm}$ at $y = 0\,\mathrm{mm}$.

Due to the finite heating rate, thermal conduction from the heated stainless steel tube into the supporting quartz glass tubes took place, extending the length of the effective hot cylinder section. The measured surface temperatures along the cylinder height at $T_S = 1000\,\mathrm{K}$ were nearly uniform at $-5\,\mathrm{mm} < y < 5\,\mathrm{mm}$, recall Fig. 4. Based on interferometry measurements near the surface, a sudden temperature drop of about 50 K occurred across the contact between stainless steel and quartz glass tubes at $y = -5\,\mathrm{mm}$ due to thermal contact resistance, and a near-linear decrease in temperature from $y = -5\,\mathrm{mm}$ ($\sim$950 K) to $y = -15\,\mathrm{mm}$ ($\sim$400 K) was observed.

A comparison of temperatures measured by interferometry at the surface, $r = 5\,\mathrm{mm}$, at $-1\,\mathrm{mm} < y < 1\,\mathrm{mm}$, and the temperature measured simultaneously by pyrometry is given in Fig. 13. Interferometry captured temperature

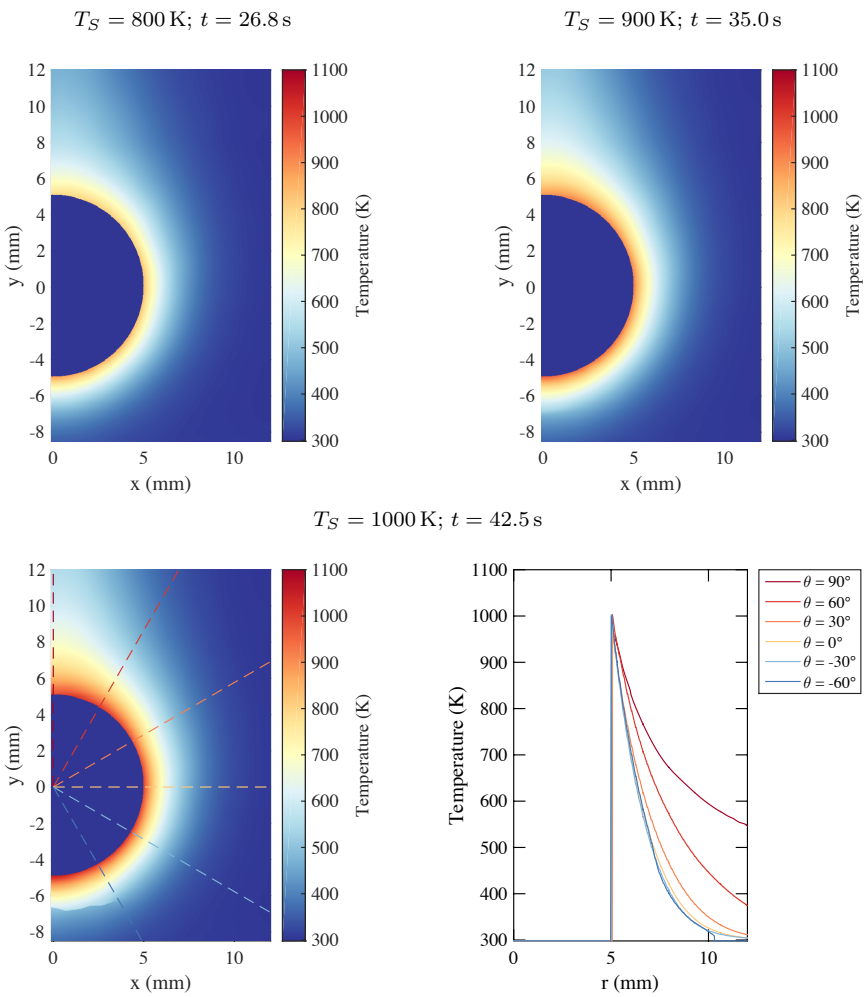

Figure 10: Gas temperature fields inferred by Fourier analysis of finite-fringe interferograms for the horizontal cylinder in stoichiometric hydrogen-air mixture. Three times corresponding to surface temperatures $T_S = [800\,\mathrm{K}; 900\,\mathrm{K}; 1000\,\mathrm{K}]$. Temperature profiles in radial coordinates for six azimuthal angles θ at $T_S = 1000\,\mathrm{K}$.

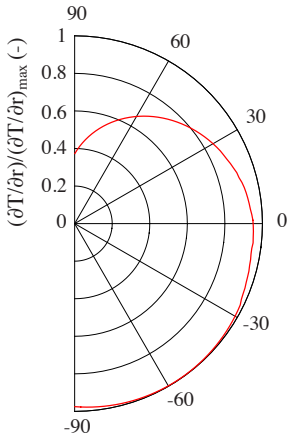

Figure 11: Evolution of local normalized wall temperature gradient about the horizontal cylinder at $T_S = 1000\,\mathrm{K}$. Qualitative analysis due to three-dimensional flow.

differences as low as about 5 K and thus the entire heating process, whereas pyrometry yielded valid measurements only at surface temperatures above about 700 K. At temperatures between 700 K and 900 K, both techniques gave equivalent results considering the pyrometry uncertainties. At higher temperatures, the scatter of interferometry measurements slightly exceeded the pyrometry uncertainty band, whereas mean values still agreed. The temperature sensitivity of interferometry decreases with increasing temperature. Overall, the agreement between both techniques provides confidence in the values of gas and surface temperature measurements reported.

6. Discussion

6.1. Comparison of ignition thresholds for hydrogen-air mixtures with previous work

Recent ignition experiments with a commercial glow plug, 5.1 mm in diameter and 9.3 mm in height, and hydrogen-air mixtures reported a near-linear increase of ignition threshold from 1010 K to 1100 K between hydrogen mole fractions of 4% and 70% and an additional increase to 1170 K towards 73% [39]. Ignition thresholds measured for hydrogen-air mixtures in the present work

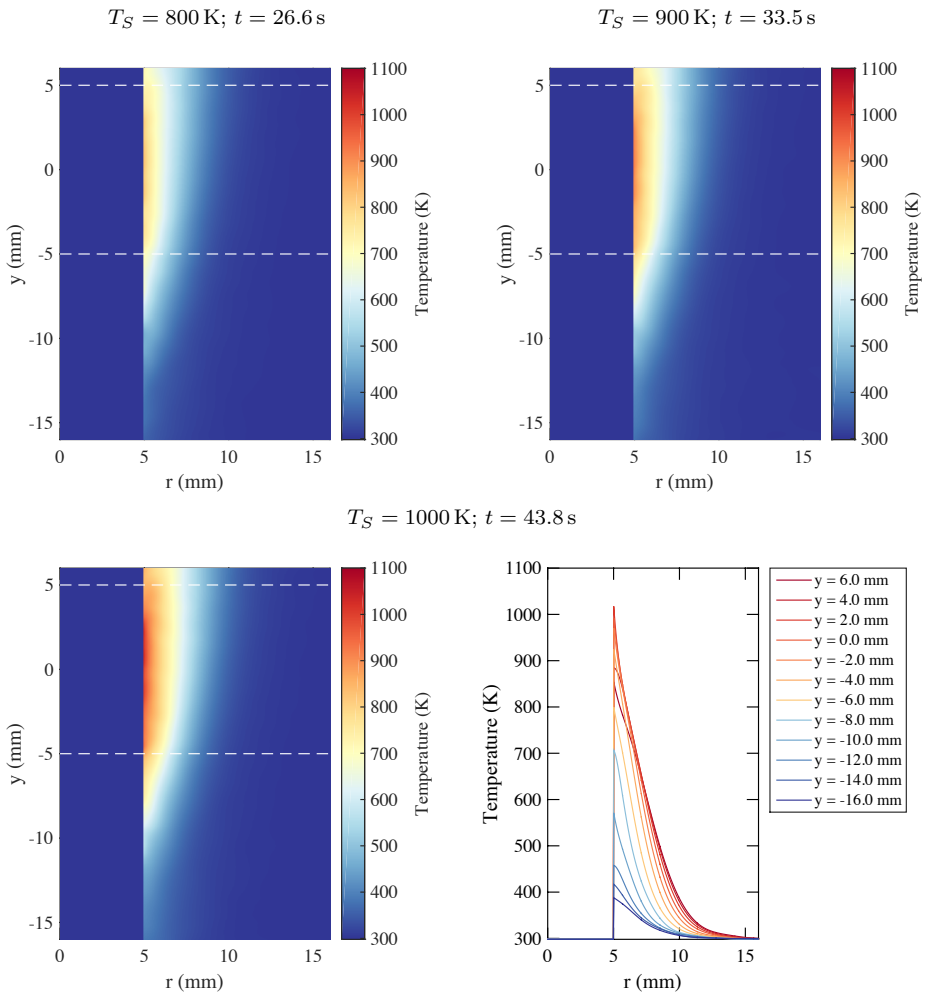

Figure 12: Gas temperature fields inferred by Fourier analysis of finite-fringe interferograms for the vertical cylinder in stoichiometric hydrogen-air mixture. Three times corresponding to surface temperatures $T_S = [800\,\mathrm{K}; 900\,\mathrm{K}; 1000\,\mathrm{K}]$. Horizontal dashed lines mark boundaries of the heated stainless steel cylinder at $y = \pm 5\,\mathrm{mm}$. Temperature profiles in radial coordinates for a range of vertical distances y at $T_S = 1000\,\mathrm{K}$.

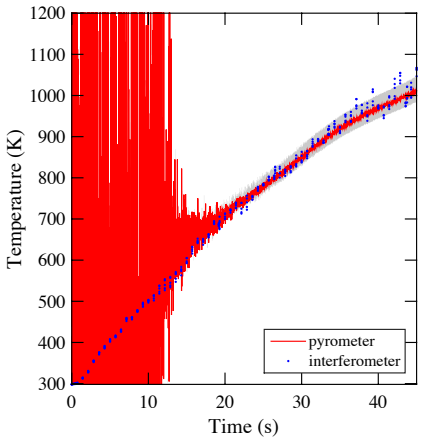

Figure 13: Comparison of temperature measurements by pyrometry and interferometry at the vertical cylinder wall, corresponding to the experiment presented in Fig. 12. Pyrometer uncertainty is given by the grey area.

range between 960 K and 1115 K and show a similar increase from lean to rich mixtures. Taking into account the measurement uncertainties, the two studies are consistent. The difference in hot surface size (glow plug height 9.3 mm and diameter 5.1 mm; heated cylinder section height 10 mm and diameter 10 mm) does not manifest in a measurable difference in ignition threshold.

6.2. Ignition in laminar boundary layers formed by free convection

A common analysis approach to describe ignition from a hot surface is to apply the Van't Hoff criterion [53] as discussed in previous work by a number of researchers, e.g. [6, 54–57]. This concept states that for ignition to take place, heat transfer due to chemical reaction within the thermal boundary layer needs to balance and exceed the heat loss from the hot surface to the gas. During the formation of a flame the temperature gradient at the surface changes sign so that heat flows from the surface to the gas prior to ignition and from the gas to the surface afterwards. The application of the Van't Hoff criterion can be simplified by assuming that (i) chemical reaction takes place in a stagnant film close to the wall and that (ii) heat transfer may be treated independently from chemical reac-

tion [6, 55, 58, 59]. Laurendeau [6] developed scaling laws for ignition in scenarios with stagnant gas, free convection and forced convection. He approached this by considering the one-dimensional, constant-density, steady-state differential equation for heat conduction, $k(d^2T/dx^2)+Qr_F = 0$, with chemical reaction rate r_F given by a single-step Arrhenius law, $r_F = -X_F^{m_F} X_O^{m_O} \rho^n A \exp[-E/(RT)]$. The symbols k, Q, X_F, X_O, m_F, m_O, n, A, E and R denote thermal conductivity, heat of combustion, fuel mole fraction, oxygen mole fraction, fuel partial order, oxygen partial order, global reaction order $n = m_F + m_O$, pre-exponential factor, activation energy and gas constant, respectively. Reactant depletion was neglected and physical properties were taken at the geometric mean temperature. Heat transfer due to chemical reaction was obtained by integrating across the thermal boundary layer. Heat loss from the surface was defined as $q_{loss} = kNu/L(T_S - T_0)$, using the Nusselt number, Nu. The Nusselt number was evaluated by Laurendeau using phenomenological models of heat transfer to non-reacting gases. In our application of this model, the Nusselt number is considered a parameter and we examine the sensitivity of the ignition temperature threshold to variations in Nu. T_0 denotes the ambient gas temperature and L is the characteristic size of the hot surface. Note that the expression for heat loss from the hot surface does not consider heat release from chemical reaction within the thermal boundary layer, see assumption (ii). Equating heat loss from the surface and heat transfer from chemical reaction for a given mixture and ambient temperature, Laurendeau obtained the following scaling law for ignition threshold $T_{S,ign}$ in a free-convection scenario:

$$\left(\frac{T_{S,ign} - T_0}{T_0}\right) T_{S,ign}^{n/2} \exp[E/(RT_{S,ign})] \propto \frac{p^n L^2}{Nu^2}. \tag{5}$$

The exponential in Eq. (5) dominates the temperature effect, so that Laurendeau simplified the ignition threshold scaling law:

$$\exp[E/(RT_{S,ign})] \propto \frac{p^n L^2}{Nu^2}. \tag{6}$$

According to this relationship, ignition from a uniformly heated surface will

always occur first at the location of smallest Nu, i.e., at the location of smallest temperature gradient such as the top edge of the vertical hot cylinder section or the upper stagnation point of the horizontal cylinder as observed in our experiments. Note that, in addition to low local heat flux, the observed ignition locations coincide with the locations of longest residence time of fluid parcels traveling within the thermal boundary layer along the hot surface. Laurendeau's model does not consider time scales of flow and chemical reaction. Recent work in our group has investigated ignition from stationary [37–39] and moving hot surfaces [31–33] using detailed numerical simulations and discussed in detail the complexity of the ignition process, analyzing, for example, individual contributions to the energy equation, the role of chemical kinetics, and effects of differential diffusion. Laurendeau's model does not consider these complexities, but it is easy to evaluate and has been widely applied. Therefore, it is useful to examine the implications to the present situation. The quantitative comparison of the predictions from realistic numerical simulations with Laurendeau's model will be the topic of future studies.

Based on Eq. (6), we define the sensitivity of ignition threshold $T_{S,ign}$ on Nu as $\Gamma = (\partial T_{S,ign}/\partial Nu)/T_{S,ign}$, for given L and p, as a function of global activation temperature E/R. We determined E/R as a function of temperature by computing constant pressure ($p = 101.3\,\mathrm{kPa}$) adiabatic explosions in Cantera [60] using detailed reaction mechanisms (hydrogen-air: [61–63]; ethylene-air: [64–66]; n-hexane-air: [38, 65, 67]) and numerically differentiating ignition delay time in Arrhenius coordinates,

$$E/R = \frac{\ln(\tau_{ign,+}) - \ln(\tau_{ign,-})}{(1/T_+) - (1/T_-)}, \tag{7}$$

where T^+ and T^- were variations of temperature by $\pm 1\%$. Ignition delay time was defined as the time to peak temperature gradient.

Figures 14–16 present the sensitivity parameter Γ and global activation tem-

perature E/R as a function of temperature for stoichiometric fuel-air mixtures. Hydrogen-air, Fig. 14, exhibits a ridge in E/R at the extended second explosion limit [68]. The predicted location of the limit in terms of temperature varies between the reaction mechanisms considered, whereas peak values of E/R are similar. For ethylene-air, Fig. 15, the mean value between all mechanisms considered is $\langle E/R \rangle_{1050-1250K} = 21{,}100\,\mathrm{K}$, with a moderate decrease with increasing temperature predicted by all mechanisms. For n-hexane-air at the present high temperatures, the global activation temperature is nearly constant, see Fig. 16, $\langle E/R \rangle_{1100-1300K} = 20{,}740\,\mathrm{K}$. Laurendeau assumed constant $E/R = 25{,}000\,\mathrm{K}$ in his analysis for methane-air. As can be seen from Figs. 14–16, all sensitivities Γ are positive, hence, ignition thresholds increase with increasing Nu. This is supported by common experience, e.g., it is known that external flow, leading to a thinner thermal boundary layer, increases ignition thresholds [18]. Likewise, a thick thermal boundary layer, such as observed locally at the horizontal cylinder upper stagnation point, enables a lower ignition threshold.

In the considered temperature ranges, the sensitivity Γ is nearly constant for n-hexane-air, shows an increase with temperature for ethylene-air, is large at high temperatures for hydrogen-air and decreases sharply toward the extended second explosion limit. The variation of cylinder orientation in our experiments had a strong effect on the local heat transfer at the observed locations of ignition as discussed in Sec. 5.3. Only ethylene-air and n-hexane-air mixtures demonstrated measurable sensitivity of ignition threshold to cylinder orientation, see Sec. 5.1. This effect is captured qualitatively by the present analysis of sensitivity parameter Γ: Ethylene-air and n-hexane-air mixtures exhibit sensitivities of about $0.1 < \Gamma < 0.2$ in the temperature regions of interest. By contrast, hydrogen-air mixture shows sensitivities as low as $\Gamma \approx 0.018$ at the extended second explosion limit ($900\,\mathrm{K} < T < 1000\,\mathrm{K}$, depending on the reaction mechanism used). At higher temperatures, sensitivities increase. The low sensitivity of hydrogen-air ignition thresholds to variatons in heat transfer, i.e., low sensitivity to cylinder orientation observed experimentally, indicates that

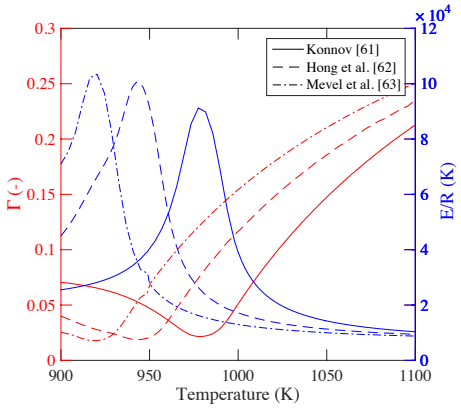

Figure 14: Ignition sensitivity parameter Γ and global activation temperature E/R for stoichiometric hydrogen-air as a function of temperature.

temperatures controlling chemical reaction within the thermal boundary layer may range around the extended second explosion limit in our hydrogen-air experiments. The present analysis reveals a limitation of Laurendeau's model for mixtures with strong variations of E/R such as hydrogen-air: Only the surface temperature is considered as a characteristic temperature and therefore the approach does not account for variations of E/R within the thermal boundary layer, and in particular around the location of ignition, slightly away from the wall.

Laurendeau's scaling model may be used for quantitative predictions of ignition threshold variations due to changes in Nu. Introducing a constant of proportionality, C, we may write Eq. (6) as

$$\exp[E/(RT_{S,ign})] = C\frac{p^n L^2}{Nu^2}. \tag{8}$$

The constant C can be determined for a known ignition threshold $T_{S,ign}$ at a reference Nusselt number Nu_{ref}. Figures 17–19 present the evolution of ignition threshold $T_{S,ign}$ due to variations in Nu. For hydrogen-air, Fig. 17, a deliberately low reference ignition threshold of 950 K has been chosen. Low Γ near the extended second explosion limit leads to small changes of $T_{S,ign}$ across

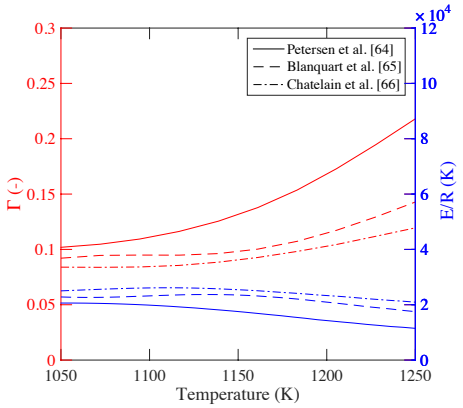

Figure 15: Ignition sensitivity parameter Γ and global activation temperature E/R for stoichiometric ethylene-air as a function of temperature.

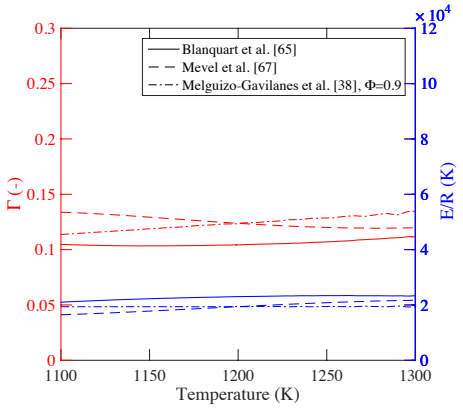

Figure 16: Ignition sensitivity parameter Γ and global activation temperature E/R for stoichiometric n-hexane-air as a function of temperature.

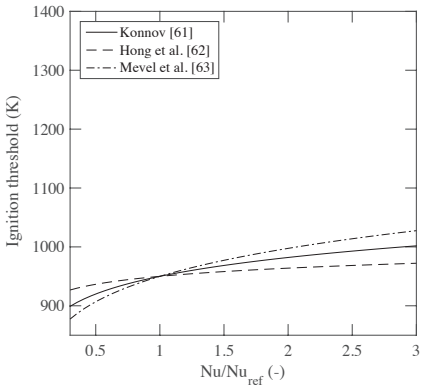

Figure 17: Variation of ignition threshold $T_{S,ign}$ with Nu for stoichiometric hydrogen-air mixture.

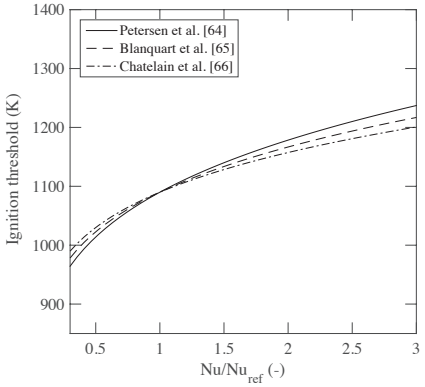

Figure 18: Variation of ignition threshold $T_{S,ign}$ with Nu for stoichiometric ethylene-air mixture.

a wide range of Nu. By contrast, ethylene-air, Fig. 18, and n-hexane-air, Fig. 19, show significantly larger variations of $T_{S,ign}$ due to larger Γ.

A thought experiment reveals the effect of the thermal plume forming above the horizontal cylinder on the ignition threshold. We ask: At what temperature would ignition take place at the lower stagnation point, where the influence of the thermal plume is negligible? We found a decrease in local temperature gradient (equivalent to a decrease in Nu) from the lower stagnation point, $\theta = -90°$,

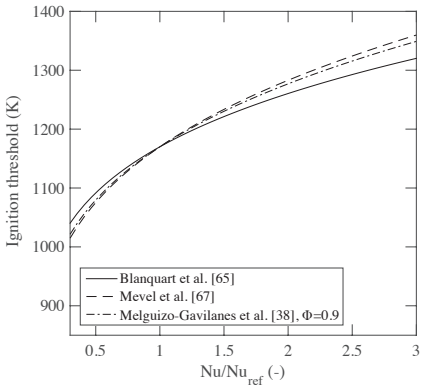

Figure 19: Variation of ignition threshold $T_{S,ign}$ with Nu for stoichiometric n-hexane-air mixture.

towards the upper stagnation point, $\theta = 90°$, by a factor of about 2.7, see Fig. 11. This value is similar to those reported in literature for comparable Rayleigh numbers on the order of 10^2–10^3, ranging between 2.8 and 3.1 [52]. Figures 17–19 demonstrate that ignition at the lower stagnation point would require higher temperatures compared to the ignition at the upper stagnation point observed in reality. The magnitude of the threshold increase depends on the fuel: For hydrogen-air, tresholds are predicted 20–70 K higher, for ethylene-air 100–130 K higher, and for n-hexane-air 130–170 K higher.

From the present experiments we did not obtain direct measurements of Nu to apply this analysis to quantitatively explain the effect of cylinder orientation on ignition threshold, due to the challenges related to the unity aspect ratio, $L/D = 1$. Based on the inspection of thermal boundary layer thickness and assuming $Nu \propto 1/\delta_{99}$, we estimate a factor in Nu between horizontal and vertical cylinder ignition locations of about 2.1. For this value, Figs. 17–19 predict differences in ignition threshold between horizontal and vertical cylinder of 15–50 K (hydrogen-air; experiment: no clear difference - note the limited applicability of Laurendeau's model for hydrogen-air due to the strong variations in E/R), 70–95 K (ethylene-air; experiment: 90 K), and 95–120 K (n-hexane-air;

experiment: 90 K). Concluding the analysis, the effect of cylinder orientation on ignition thresholds can be explained by changes in convection pattern under the influence of chemical mixture properties.

7. Conclusions

We experimentally studied the ignition of fuel-air mixtures from a heated circular cylinder situated inside a closed combustion vessel, considering initially quiescent hydrogen-air, ethylene-air and n-hexane-air mixtures over a wide range of equivalence ratio at initial pressure and temperature of 101.3 kPa and 296 K, respectively. A hot surface with a cylindrical cross-section and a unity aspect ratio, $L = D = 10$ mm, was designed to provide a region of spatially uniform temperature. Separate experiments with vertical and horizontal cylinder orientation were conducted. For each test, the cylinder was heated from room temperature up to surface temperatures for ignition. Ignition thresholds, i.e., the temperatures of the hot surface at the time of ignition, were measured by two-color pyrometry. High-speed digital video recording of Mach-Zehnder interferometry enabled the visualization of ignition dynamics, gas temperature fields and computations of heat transfer parameters.

In a stoichiometric hydrogen-air mixture, ignition occurred at temperatures around 1050 K. Variation of the cylinder orientation did not lead to a clear change in threshold. By contrast, ethylene-air and n-hexane-air mixtures showed pronounced sensitivity of ignition threshold on cylinder orientation: For both fuels, thresholds were higher for the vertical orientation than for horizontal. Stoichiometric ethylene-air mixture ignited at about 1090 K for the horizontal cylinder and at about 1180 K for the vertical cylinder; stoichiometric n-hexane-air mixture ignited at about 1180 K for the horizontal cylinder and at about 1270 K for the vertical cylinder. The dependence of ignition threshold on equivalence ratio was less than 100 K across the range studied: Thresholds increased from lean to rich for hydrogen-air, decreased from lean to rich for ethylene-air

and remained nearly constant for n-hexane-air.

Ignition was found to take place consistently at the top (upper stagnation point) of the horizontal cylinder and near the upper edge of the heated section of the vertical cylinder. These ignition locations coincided with the locations of lowest local wall heat flux (thickest thermal boundary layer) and long residence time of gas parcels traveling within the thermal boundary layer.

An analytical scaling model for ignition from hot surfaces by Laurendeau was applied to evaluate the sensitivity of ignition thresholds to variations in local heat transfer about the hot surface for the three fuels. The analysis revealed a low sensitivity for hydrogen-air mixtures at temperatures near the extended second explosion limit, where global activation temperature is high. Sensitivities for ethylene-air and n-hexane-air were higher, which qualitatively reproduces the experimental observations from horizontal and vertical cylinder experiments.

Acknowledgements

The present work was carried out in the Explosion Dynamics Laboratory of the California Institute of Technology and was supported by The Boeing Company through a Strategic Research and Development Relationship Agreement CT-BA-GTA-1. The authors thank Dr. Stephanie Coronel for her contributions to the Fourier analysis of interferograms.

References

[1] H. P. Stout, E. Jones, The ignition of gaseous explosive media by hot wires, Symposium on Combustion and Flame, and Explosion Phenomena (1948) 329–336.

[2] S. Kumagai, I. Kimura, Ignition of flowing gases by heated wires, Symp. (Int.) Combust. 6 (1957) 554–558.

[3] L. E. Ashman, A. Büchler, The ignition of gases by electrically heated wires, Combust. Flame 5 (1961) 113–121.

[4] J. M. Kuchta, A. Bartkowiak, M. G. Zabetakis, Hot surface ignition temperatures of hydrocarbon fuel vapor–air mixtures, J. Chem. Eng. Data 10 (1965) 282–288.

[5] C. M. Detz, Threshold conditions for the ignition of acetylene gas by a heated wire, Combust. Flame 26 (1976) 45–55.

[6] N. M. Laurendeau, Thermal ignition of methane–air mixtures by hot surfaces: A critical examination, Combust. Flame 46 (1982) 29–49.

[7] N. M. Laurendeau, R. N. Caron, Influence of hot surface size on methane–air ignition temperature, Combust. Flame 46 (1982) 213–218.

[8] R. K. Kumar, Ignition of hydrogen–oxygen–diluent mixtures adjacent to a hot, nonreactive surface, Combust. Flame 75 (1989) 197–215.

[9] N. B. Siccama, K. R. Westerterp, The explosion region becomes smaller under flow conditions: the ignition of ethene–air mixtures with a hot surface, Ind. Eng. Chem. Res. 32 (1993) 1304–1314.

[10] H. Nagata, H. M. Kim, J. Sato, M. Kono, An experimental and numerical investigation on the hot surface ignition of premixed gases under microgravity conditions, Symp. (Int.) Combust. 25 (1994) 1719–1725.

[11] J. W. Buckel, S. Chandra, Hot wire ignition of hydrogen–oxygen mixtures, Int. J. Hydrogen Energ. 21 (1996) 39–44.

[12] H. M. Kim, H. Enomoto, H. Kato, M. Kono, Effects of natural convection and catalytic reaction on the hot surface ignition of methane–air mixtures, KSME/JSME THERMAL and FLUID Engineering Conference (1996) 319–324.

[13] H. M. Kim, H. Enomoto, H. Kato, M. Tsue, M. Kono, A study of the ignition mechanism of methane–air mixtures by inert and catalytic hot surfaces, Combust. Sci. Technol. 128 (1997) 197–213.

[14] H. M. Kim, H. Enomoto, H. Kato, M. Tsue, M. Kono, The effect of catalytic reaction on hot surface ignition, JSME Int. J. B-Fluid T. 41 (1998) 945–950.

[15] D. Oancea, D. Razus, M. Mitu, S. Constantinesco, Hot wire ignition of premixed flammable fuel-air mixtures using isothermally heated platinum wires, Rev. Roum. Chim. 47 (2002) 91–97.

[16] P. Stathopoulos, K. Ninck, P. R. von Rohr, Hot-wire ignition of ethanol–oxygen hydrothermal flames, Combust. Flame 160 (2013) 2386–2395.

[17] H. F. Coward, P. G. Guest, Ignition of natural gas–air mixtures by heated metal bars, J. Am. Chem. Soc. 49 (1927) 2479–2486.

[18] J. W. Mullen, J. B. Fenn, M. R. Irby, The ignition of high velocity streams of combustible gases by heated cylindrical rods, Symposium on Combustion and Flame, and Explosion Phenomena (1948) 317–329.

[19] G. Adomeit, Ignition of gases at hot surfaces under nonsteady–state conditions, Symp. (Int.) Combust. 10 (1965) 237–243.

[20] D. P. Cutler, The ignition of gases by rapidly heated surfaces, Combust. Flame 22 (1974) 105–109.

[21] D. P. Cutler, Further studies of the ignition of gases by transiently heated surfaces, Combust. Flame 33 (1978) 85–91.

[22] K. C. Smyth, N. P. Bryner, Short-duration autoignition temperature measurements for hydrocarbon fuels near heated metal surfaces, Combust. Sci. Technol. 126 (1997) 225–253.

[23] R. S. Silver, The ignition of gaseous mixtures by hot particles, Lond. Edinb. Dubl. Phil. Mag. 23 (1937) 633–657.

[24] S. Paterson, I. The ignition of inflammable gases by hot moving particles, Lond. Edinb. Dubl. Phil. Mag. 28 (1939) 1–23.

[25] S. Paterson, II. The ignition of inflammable gases by hot moving particles, Lond. Edinb. Dubl. Phil. Mag. 30 (1940) 437–457.

[26] T. H. Dubaniewicz, K. L. Cashdollar, G. M. Green, R. F. Chaiken, Ignition of methane–air mixtures by laser heated small particles, J. Loss Prevent. Proc. 13 (2000) 349–359.

[27] T. H. Dubaniewicz, Threshold powers and delays for igniting propane and butane-air mixtures by cw laser–heated small particles, J. Laser Appl. 18 (2006) 312–319.

[28] M. Beyer, D. Markus, Ignition of explosive atmospheres by small hot particles: Comparison of experiments and simulations, Sci. Technol. Energ. Ma. 73 (2012) 1–7.

[29] D. Roth, P. Sharma, T. Haeber, R. Schiessl, H. Bockhorn, U. Maas, Ignition by mechanical sparks: ignition of hydrogen/air mixtures by submillimeter–sized hot particles, Combust. Sci. Technol. 186 (2014) 1606–1617.

[30] D. Roth, T. Haeber, H. Bockhorn, Experimental and numerical study on the ignition of fuel/air mixtures at laser heated silicon nitride particles, Proc. Combust. Inst.doi:http://dx.doi.org/10.1016/j.proci.2016.05.054.

[31] S. A. Coronel, Thermal ignition using moving hot particles, Ph.D. thesis, California Institute of Technology (2016).

[32] J. Melguizo-Gavilanes, S. Coronel, R. Mével, J. E. Shepherd, Dynamics of ignition of stoichiometric hydrogen–air mixtures by moving heated particles, Int. J. Hydrogen Energ.doi:http://dx.doi.org/10.1016/j.ijhydene.2016.05.206.

[33] J. Melguizo-Gavilanes, R. Mével, S. Coronel, J. E. Shepherd, Effects of differential diffusion on ignition of stoichiometric hydrogen–air by moving hot spheres, Proc. Combust. Inst.doi:http://dx.doi.org/10.1016/j.proci.2016.06.120.

[34] P. A. Boettcher, Thermal ignition, Ph.D. thesis, California Institute of Technology (2012).

[35] P. A. Boettcher, S. K. Menon, B. L. Ventura, G. Blanquart, J. E. Shepherd, Cyclic flame propagation in premixed combustion, J. Fluid Mech. 735 (2013) 176–202.

[36] S. K. Menon, P. A. Boettcher, B. Ventura, G. Blanquart, Hot surface ignition of n-hexane in air, Combust. Flame 163 (2016) 42–53.

[37] J. Melguizo-Gavilanes, L. R. Boeck, R. Mével, J. E. Shepherd, Hot surface ignition of stoichiometric hydrogen–air mixtures, Int. J. Hydrogen Energ.doi:http://dx.doi.org/10.1016/j.ijhydene.2016.05.095.

[38] J. Melguizo-Gavilanes, A. Nové-Josserand, S. Coronel, R. Mével, J. E. Shepherd, Hot surface ignition of n–hexane mixtures using simplified kinetics, Combust. Sci. Technol. 188 (2016) 2060–2076. doi:http://dx.doi.org/10.1080/00102202.2016.1212577.

[39] R. Mével, J. Melguizo-Gavilanes, L. Boeck, J. Shepherd, Experimental and numerical study of the ignition of hydrogen-air mixtures by a localized stationary hot surface. Article submitted to Combust. Flame 03/2017.

[40] I. O. Wilson, Magnesium oxide as a high–temperature insulant, IEE Proceedings A-Physical Science, Measurement and Instrumentation, Management and Education-Reviews 128 (1981) 159–164.

[41] P. B. Coates, Multi–wavelength pyrometry, Metrologia 17 (1981) 103.

[42] C. M. Vest, Holographic interferometry, John Wiley and Sons, New York, 1979.

[43] W. C. Gardiner, Y. Hidaka, T. Tanzawa, Refractivity of combustion gases, Combust. Flame 40 (1981) 213–219.

[44] F. J. Weinberg, Optics of flames, Butterworth & Co. Ltd., London, 1963.

[45] P. Rastogi, E. Hack, Phase estimation in optical interferometry, CRC Press, 2014.

[46] D. C. Ghiglia, M. D. Pritt, Two-dimensional phase unwrapping: theory, algorithms, and software, Vol. 4, Wiley New York, 1998.

[47] Q. Kemao, Windowed fourier transform for fringe pattern analysis, Appl. Optics 43 (2004) 2695–2702.

[48] Q. Kemao, Windowed fringe pattern analysis, SPIE Press Bellingham, Wash, USA, 2013.

[49] G. Pretzler, A new method for numerical Abel-inversion, Zeitschrift für Naturforschung 46 (1991) 639–641.

[50] L. D. Landau, E. M. Lifshitz, Fluid mechanics, Pergamon Press Ltd, 1987.

[51] M. J. Hurley, D. T. Gottuk, J. R. Hall Jr, K. Harada, E. D. Kuligowski, M. Puchovsky, J. M. Watts Jr, C. J. Wieczorek, et al., SFPE handbook of fire protection engineering, Springer, 2015.

[52] S. Boetcher, Natural convection from circular cylinders, Springer, 2014.

[53] J. H. Van't Hoff, Studies in Chemical Dynamics, Williams and Norgate, London, 1896.

[54] A. Alkidas, P. Durbetaki, Ignition of a gaseous mixture by a heated surface, Combust. Sci. Technol. 7 (1973) 135–140.

[55] A. Alkidas, P. Durbetaki, A simplified model for stagnation heat transfer and ignition of a gaseous mixture, J. Heat Transf. 95 (1973) 564–566.

[56] C. K. Law, On the stagnation-point ignition of a premixed combustible, Int. J. Heat Mass Tran. 21 (1978) 1363–1368.

[57] L. D. Chen, G. M. Faeth, Ignition of a combustible gas near heated vertical surfaces, Combust. Flame 42 (1981) 77–92.

[58] L. N. Khitrin, S. A. Goldenberg, Thermal theory of ignition of gas mixtures: Limiting conditions, Symp. (Int.) Combust. 6 (1957) 545–554.

[59] A. G. Merzhanov, A. E. Averson, The present state of the thermal ignition theory: An invited review, Combust. Flame 16 (1971) 89–124.

[60] D. G. Goodwin, H. K. Moffat, R. L. Speth, Cantera: An object-oriented software toolkit for chemical kinetics, thermodynamics, and transport processes, version 2.2.1 (2016).
URL `http://www.cantera.org`

[61] A. A. Konnov, Remaining uncertainties in the kinetic mechanism of hydrogen combustion, Combust. Flame 152 (2008) 507–528.

[62] Z. Hong, D. F. Davidson, R. K. Hanson, An improved h_2/o_2 mechanism based on recent shock tube/laser absorption measurements, Combust. Flame 158 (2011) 633–644.

[63] R. Mével, S. Javoy, F. Lafosse, N. Chaumeix, G. Dupré, C. E. Paillard, Hydrogen-nitrous oxide delay time: shock tube experimental study and kinetic modelling, Proc. Combust. Inst. 32 (2009) 359–366.

[64] E. L. Petersen, D. M. Kalitan, S. Simmons, G. Bourque, H. J. Curran, J. M. Simmie, Methane/propane oxidation at high pressures: Experimental and detailed chemical kinetic modeling, Proc. Combust. Inst. 31 (2007) 447–454.

[65] G. Blanquart, P. Pepiot-Desjardins, H. Pitsch, Chemical mechanism for high temperature combustion of engine relevant fuels with emphasis on soot precursors, Combust. Flame 156 (2009) 588–607.

[66] K. Chatelain, R. Mével, S. Menon, G. Blanquart, J. E. Shepherd, Ignition and chemical kinetics of acrolein-oxygen-argon mixtures behind reflected shock waves, Fuel 135 (2014) 498–508.

[67] R. Mével, K. Chatelain, P. A. Boettcher, G. Dayma, J. E. Shepherd, Low temperature oxidation of n-hexane in a flow reactor, Fuel 126 (2014) 282–293.

[68] R. A. Yetter, H. Rabitz, R. M. Hedges, A combined stability-sensitivity analysis of weak and strong reactions of hydrogen/oxygen mixtures, Int. J Chem. Kinet. 23 (1991) 251–278.